JOURNAL OF CATALYSIS **180,** 161–170 (1998)
ARTICLE NO. CA982270

Isolation of Active Adsorbates for the NO–CO Reaction on Pd/Al_2O_3 by Selective Enhancement and Selective Poisoning

Khalid Almusaiteer and Steven S. C. Chuang[1]

Department of Chemical Engineering, The University of Akron, Akron, Ohio 44325-3906

Received February 16, 1998; revised August 26, 1998; accepted August 31, 1998

A novel experimental approach which couples *in situ* infrared (IR) with selective enhancement and poisoning has been developed to identify the active adsorbate for the NO–CO reaction on Pd/Al_2O_3. *In situ* IR studies of the steady-state NO–CO reaction show that NO adsorbs as Pd–N≡O$^{\delta+}$, Pd–N=O, and Pd–N$^{\diagup O^{\delta-}}$; CO adsorbs as Pd–C≡O and $^{Pd}_{Pd}$>C=O. Addition of H_2 to the NO–CO flow as a reaction enhancer which reacts with adsorbed nitrogen and oxygen results in depletion of Pd–N=O, while addition of O_2 to the NO–CO flow as a reaction poison leads to accumulation of Pd–N=O on the Pd surface. These observations suggest that Pd–N=O is the active adsorbate involved in NO dissociation. The observed variation in the concentrations of CO_2 and Pd–C≡O suggests that Pd–C≡O is the active adsorbate leading to CO_2. This study demonstrates that combined *in situ* IR with careful selection of enhancing and poisoning reagents allows unambiguous identification of active adsorbates under reaction conditions.

INTRODUCTION

Knowledge of the structure and reactivity of adsorbates is the key to developing a fundamental understanding of the reaction mechanism on the catalyst surface (1–3). Various spectroscopic techniques have been developed to determine the structure of adsorbates on the catalyst surface. The most widely used technique for determining the structure of adsorbates on supported metal catalysts is *in situ* infrared (IR) spectroscopy, which measures both active and spectator adsorbates (4–8). The former participates in the catalytic cycle leading to product formation; the latter is not involved in the reaction.

Discriminating between active adsorbates and spectators has been a challenging subject in fundamental catalysis research. Reactive adsorbates may be distinguished from spectators by comparing the transient responses of adsorbates resulting from a perturbation in reactant and its isotope concentration, temperature, and pressure (1–3, 9–11). Strong dependence of adsorbate reactivity on reaction conditions requires that the reactivity of adsorbate be measured under reaction environment where all reactants and products are present. One approach to studying the adsorbate transients under reaction conditions is the steady-state isotopic transient kinetic analysis (SSITKA) (12–15), which involves replacing a reactant flow by its isotopically labeled counterpart in the form of a step function to the inlet of an *in situ* IR reactor. The use of this technique to study the NO–CO reaction on Rh/SiO_2 has allowed identification of Rh–NCO as a spectator for CO_2 formation and has revealed the occurrence of a rapid exchange (i.e., adsorption and desorption) between gaseous and adsorbed CO (12). This rapid exchange between gaseous and adsorbed reactants precludes use of the SSITKA to determine the modes of adsorbed CO and NO participating in the NO–CO reaction.

In this paper, we present a novel approach to distinguish active adsorbates from spectator adsorbates by combining *in situ* IR with selective enhancement and poisoning techniques. An enhancing or poisoning agent can be carefully selected to accelerate a specific reaction that depletes the active adsorbate or to inhibit such a reaction that results in accumulation of the active adsorbate. Application of this novel concept to the identification of active NO adsorbates for the NO–CO reaction is illustrated in Fig. 1. The schematic in Fig. 1a provides the proposed pathway for the catalytic NO–CO reaction (16–18). CO_2 formation from NO and CO involves the reaction of adsorbed CO with adsorbed oxygen which results from dissociated NO. N_2 formation involves a combination of adsorbed nitrogen atoms produced from NO dissociation. Although the reaction pathway in Fig. 1 appears to be straightforward, fundamental questions have yet to be addressed such as (i) what types of NO and CO adsorbates (i.e., cationic NO, linear NO, bent NO, linear CO, and bridged CO) participate in the catalytic NO–CO reaction and (ii) which step is rate-limiting.

Figures 1b and 1c illustrate the approach of selective enhancement of the NO–CO reaction with the addition of hydrogen and selective poisoning of the reaction with the addition of oxygen, respectively. Since the dissociation of adsorbed NO (i.e., Pd–NO + Pd → Pd–N + Pd–O) requires

[1] To whom correspondence should be addressed.

0021-9517/98 $25.00

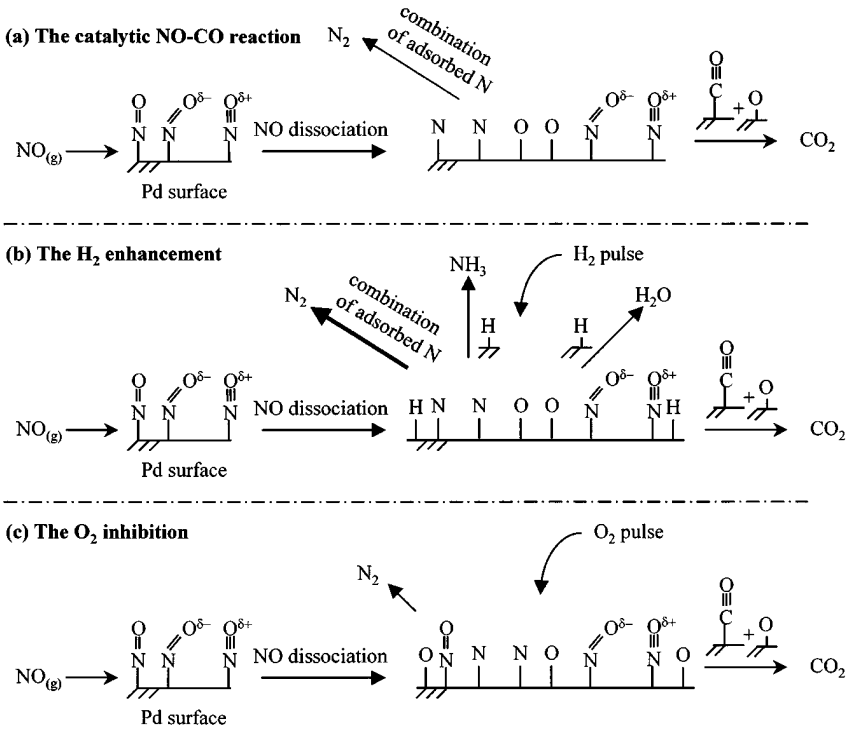

FIG. 1. (a) The proposed NO–CO reaction pathway. (b) Selective enhancement causes a decrease in the concentration of active adsorbate. (c) Selective poisoning causes an increase in the concentration of active adsorbate.

an empty neighboring Pd site, removal of adsorbed oxygen (Pd–O) by the addition of hydrogen may promote the dissociation of adsorbed NO, increasing NO conversion; the addition of oxygen may inhibit NO dissociation, decreasing NO conversion. The former should decrease the concentration of active NO adsorbates involved in NO dissociation. The latter may either increase or decrease the concentration of active NO adsorbates, depending on the role of added oxygen in NO adsorption and dissociation. Enhancement and poisoning of the NO–CO reaction were carried out by the pulse injection of H_2 and O_2 into the steady-state NO/CO flow on Pd/Al_2O_3. Variation in concentration of adsorbates as well as those of gaseous reactants and products was monitored by Fourier transform infrared (FTIR) spectroscopy and mass spectrometry (MS), respectively.

EXPERIMENTAL

The Pd/Al_2O_3 catalyst was prepared by incipient-wetness impregnation of γ-Al_2O_3 support (Alfa Chemicals, 100 m^2/g) with a $PdCl_2$ (Alfa Chemicals) solution at a pH of 2.8 and 60°C (19). The ratio of solution to weight of Al_2O_3 was 1 cm^3 to 1 g. The catalyst was calcined in flowing air at 673 K for 8 h and then reduced in flowing H_2 at 673 K for 8 h. The Pd loading of Pd/Al_2O_3 was determined to be 1.75 wt% by inductively coupled plasma (ICP) analysis (Galbraith Laboratories, Inc.). The dispersion of Pd atoms in the reduced catalyst, determined by H_2 pulse chemisorption at room temperature, was 16% corresponding to the average Pd crystallite size of 60 Å. The hydrogen pulse chemisorption only measure irreversibly adsorbed hydrogen. The X-ray diffraction (XRD) technique was applied to further confirm the Pd crystallite size and Pd dispersion. The Pd average crystallite size, determined by XRD, was 64 Å, corresponding to a dispersion of 13%.

The catalyst was pressed into three self-supporting disks for the *in situ* transmission IR studies. Prior to the adsorption and reaction experiments, the catalyst was further reduced *in situ* at 673 K for 2 h. Details of the experimental apparatus have been presented elsewhere (20) and will be briefly discussed here. The experimental system consists of (i) the gas flow system with a six-port pulsing valve, (ii) the *in situ* IR reactor cell with self-supporting catalyst disks, and (iii) the analysis section with MS and gas chromatography (GC). Flows of NO/CO/He (3/9/28 cm^3/min) to the IR reactor cell were controlled by mass flow controllers. Figure 2a shows that the six-port valve allows injection of 10 cm^3 of H_2 into the NO/CO/He reactant stream. To avoid the reaction of NO with O_2 in the transportation lines at room temperature, O_2 was injected into the He flow, which was further mixed with NO/CO in the heated IR reactor cell, as shown in Fig. 2b.

The steady-state and transient IR spectra were collected by a Nicolet magna-IR 550 spectrometer equipped with a

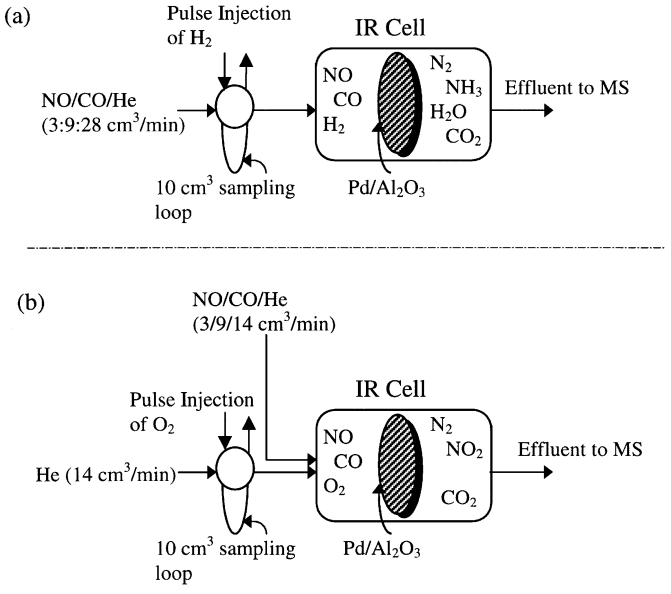

FIG. 2. Experimental approaches (a) H_2 pulse injection and (b) O_2 pulse injection.

MCT-B detector at a resolution of 4 cm^{-1}. The effluent gases of the IR reactor cell were monitored by a Balzers QMG112 mass spectrometer. The gaseous responses for m/e ratios corresponding to CO and N_2 ($m/e=28$), NO ($m/e=30$), and CO_2 and N_2O ($m/e=44$) were monitored by the MS. The CO_2 and N_2O ($m/e=44$) responses can be separated by using the response ratio of the primary ionization ($m/e=44$) and the secondary ionization ($m/e=22$) of CO_2. The ratio of the $m/e=44$ peak to the $m/e=22$ peak for CO_2 was found to be 50.8 by the injection of a known amount of CO_2 into the helium carrier. An HP-5890A gas chromatograph with a TCD detector was used to measure the steady-state NO, CO, and N_2 concentration in the effluent of the IR reactor cell.

RESULTS

Steady-State NO, CO, and NO/CO Flow

Figure 3 shows the IR spectra of individual NO and CO adsorbates at different temperatures. The catalyst was reduced at 673 K prior to exposure to NO, CO, and NO–CO flows. Gaseous CO and NO bands are also presented in Fig. 3, which show the extent of overlapping of their adsorbate bands. Assignment of 1780 cm^{-1} to cationic NO (Pd–N≡O$^{\delta+}$), 2062 cm^{-1} to linear CO (Pd–C≡O), and 1929 and 1862 cm^{-1} to bridged CO ($^{Pd}_{Pd}$>C=O) has been well established in the literature (19, 21–30). The 1685 cm^{-1} band may be assigned to a bridged NO ($^{Pd}_{Pd}$>N=O), a bent NO (Pd–N$^{\diagup O^{\delta-}}$), or a linear, highly back-bonded NO species (19). Recent studies on Ag–Pd/SiO_2 catalyst exclude the assignment of the 1685 cm^{-1} band to $^{Pd}_{Pd}$>N=O based on the blocking effect of Ag on bridged NO sites (26). Due to considerable overlap of IR bands of various adsorbates and the lack of decisive techniques to determine the adsorbate structure, we tentatively assign the 1685 cm^{-1} band to a Pd–N$^{\diagup O^{\delta-}}$ species.

Figure 3a shows that exposure of the catalyst to the steady-state flow of NO/He (10/30 cm^3/min) produced

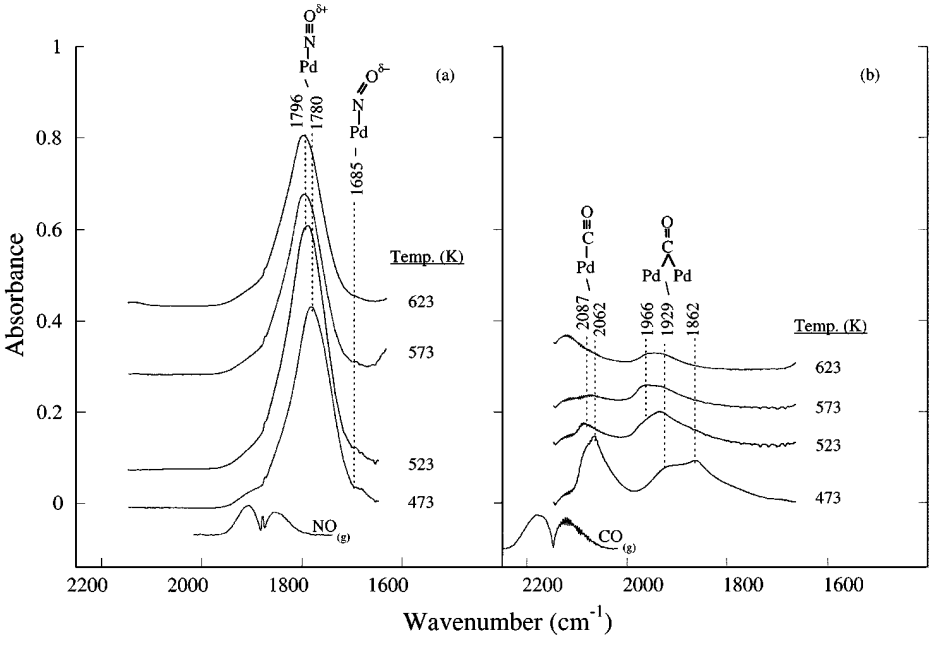

FIG. 3. (a) IR spectra during the steady-state NO/He (10/30 cm^3/min) flow at different temperatures. (b) IR spectra during the steady-state CO/He flow (10/30 cm^3/min) at different temperatures.

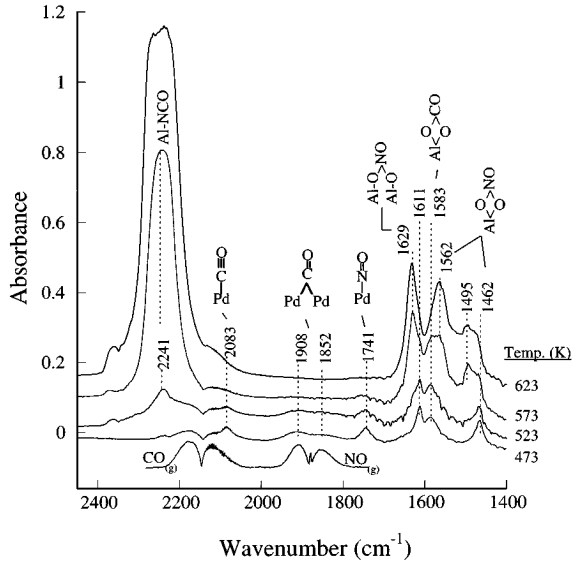

FIG. 4. IR spectra during the steady-state NO/CO/He (3/9/28 cm^3/min) flow at different temperatures.

Pd–N≡O$^{\delta+}$ at 1780 cm^{-1} and Pd–N$^{O^{\delta-}}$ at 1685 cm^{-1}. Increasing temperature caused a slight decrease in the intensity of the Pd–N≡O$^{\delta+}$ species with a shift in its wavenumber to 1796 cm^{-1}. Exposure of the catalyst to the steady-state CO/He (10/30 cm^3/min) flow produced Pd–C≡O at 2062 cm^{-1} and $^{Pd}_{Pd}$>C=O at 1929 and 1862 cm^{-1}. Increasing the temperature to 623 K resulted in bridged CO being the only species on the Pd surface.

Figure 4 shows that flowing NO/CO/He over the catalyst at different temperatures produced Pd–C≡O at 2083 cm^{-1}, $^{Pd}_{Pd}$>C=O at 1908 and 1852 cm^{-1}, and linear NO (Pd–N=O) at 1741 cm^{-1} as well as carbonate and bidentate nitrato on Al_2O_3 in the 1400–1629 cm^{-1} region. The assignment of the latter bands to the species shown in Fig. 4 is based on individual adsorption of NO and CO on the Al_2O_3 surface. The overall shape of the band at ca. 1900 cm^{-1} is due to the overlap of IR bands of both $^{Pd}_{Pd}$>C=O and gaseous NO. Increasing temperature caused a decrease in the IR intensity of CO and NO adsorbates on the Pd surface, but an increase in that of the carbonate and bidentate nitrato species on the Al_2O_3 surface. Table 1 shows that increasing temperature causes an increase in the NO and CO conversion. Temperature-programmed reaction (TPR) study showed that the light-off occurred at about 580 K. At 623, i.e., above the light-off temperature, both Pd–C≡O and $^{Pd}_{Pd}$>C=O as well as Pd–N=O intensity attenuated to a negligible level. The drop in intensity of NO and CO adsorbates on Pd surface is in sharp contrast with the observation of intense Pd–N≡O$^{\delta+}$ and $^{Pd}_{Pd}$>C=O bands in Fig. 3 when the reactants were flowed individually over the catalyst. The observation of Pd–N≡O$^{\delta+}$ during the individual NO flow and that of Pd–N=O during the NO–CO reaction suggest a strong dependence of Pd oxidation state on the reactant environment, where the presence of CO under the NO–CO reaction conditions keeps Pd in the reduced state for catalyzing the reaction. The absence of strong Pd–N=O and Pd–C≡O bands accompanied by high NO and CO conversion at 623 K suggests that the surface reaction rapidly depleted the adsorbed NO and CO on the Pd surface. Mass transfer limitations may not allow the gaseous NO and CO to reach the Pd surface rapidly enough to offset the consumption of adsorbed NO and CO by the reaction. The appearance of prominent isocyanate species (Al–NCO) as well as carbonate and nitrato bands observed at temperatures above 573 K reflects that their formation rates are greater than their destruction rates at elevated temperatures.

Pulse H_2 into NO/CO/He Flow

Figure 5a shows the IR spectra obtained during the pulse injection of 10 cm^3 hydrogen into the NO/CO/He (3/9/30 cm^3/min) steady-state flow at 473 K. The initial spectrum during the steady-state NO/CO/He flow showed Pd–C≡O at 2080 cm^{-1}, $^{Pd}_{Pd}$>C=O at 1922 and 1852 cm^{-1}, Pd–N=O at 1748 cm^{-1}, and bidentate nitrato and carbonate species in the 1611–1466 cm^{-1} region. Pulse injection of H_2 caused the following changes: (i) an increase in the intensity of NH_3 at 3195 cm^{-1} (29), (ii) a growth in the intensities of Pd–C≡O and $^{Pd}_{Pd}$>C=O, (iii) a reduction in the intensity of Pd–N=O, (iv) an emergence of a Pd–N$^{O^{\delta-}}$ band at 1682 cm^{-1}, and (v) a variation in the carbonate and nitrato intensity. The variation in IR intensity of CO and NO on Pd is further highlighted by the difference spectra in Fig. 5b. Positive bands indicate an increase in IR intensity with respect to the initial spectrum and vice versa for negative bands.

Changes in the integrated IR intensity as a function of time are plotted along with variation in the effluent composition in Fig. 6. Decrease in the IR intensity of Pd–N=O was accompanied by an increase in Pd–C≡O at 2080 cm^{-1} and N_2O at 2234 cm^{-1} as well as in MS intensity of CO/N_2 ($m/e=28$), NH_3 ($m/e=17$), H_2O ($m/e=18$), NO ($m/e=30$), CO_2 and N_2O. Increase in MS intensity of N_2O, NH_3, H_2O, and CO_2 indicates an increase in their formation rates, while the decrease in MS intensity of NO reflects an increase in NO conversion. Pairing the decrease in reactant and adsorbate concentration with the increase

TABLE 1

Conversion Obtained by GC Analysis during the Steady-State NO/CO/He Flow on Pd/Al_2O_3

	Conversion (%)	
Temperature (K)	NO	CO
473	29	20
523	36	23
573	39.4	34
623	88.7	83

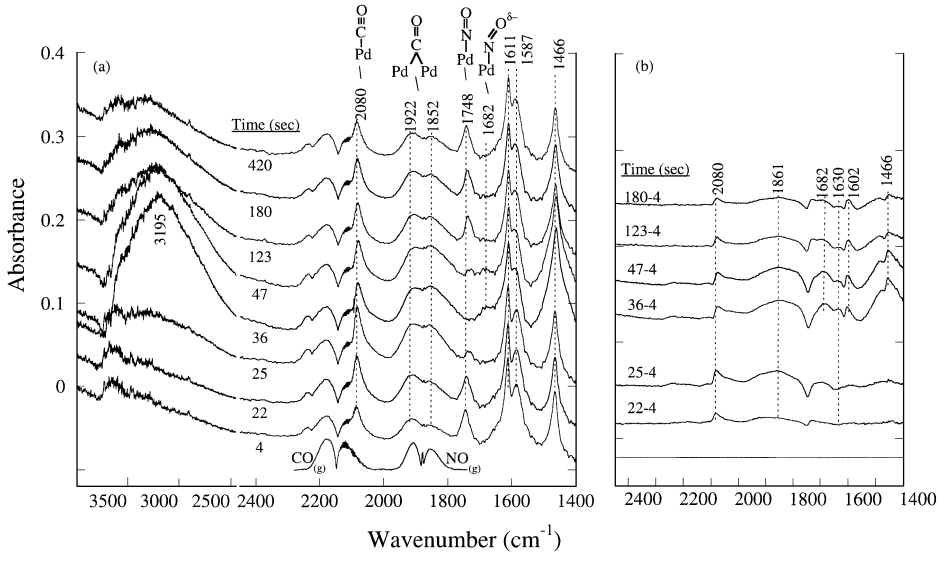

FIG. 5. (a) Transient IR spectra of adsorbed species during the 10 cm^3 H_2 pulse into the flow of NO/CO/He (3/9/28 cm^3/min) at 473 K. (b) The difference spectra are obtained by the subtraction of the first spectrum from subsequent spectrum (e.g., spectrum at 22-4 resulted from the difference between spectra at 22 and 4 s; spectrum at 180-4 resulted from the difference between spectra at 180 and 4 s).

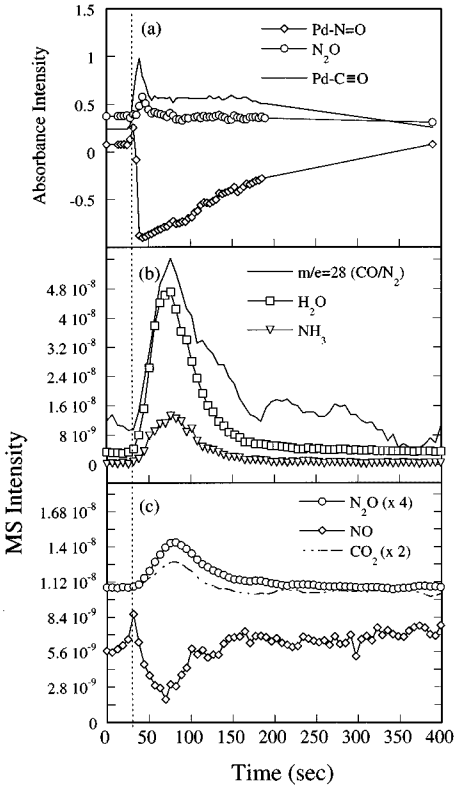

FIG. 6. (a) Integrated absorbance intensity as a function of time obtained from $\bar{A}_{N_2O} = \int_{2229}^{2271} A(v)\,dv$, $\bar{A}_{Pd-C\equiv O} = \int_{2053}^{2105} A(v)\,dv$, and $\bar{A}_{Pd-N=O} = \int_{1720}^{1776} A(v)\,dv$, where A_i is the integrated absorbance intensity for *i* species. (b, c) MS intensity profiles of effluent from the reactor in Fig. 5 as a function of time.

in product concentration in the reactor effluent suggests the occurrence of the following reactions:

H_2 adsorption	$H_2 + 2Pd \rightarrow 2Pd–H$	[1]
NO dissociation	$Pd–NO + Pd \rightarrow Pd–N + Pd–O$	[2]
H_2O formation	$Pd–H + Pd–O \rightarrow Pd–OH + Pd$	[3]
	$Pd–OH + Pd–H \rightarrow H_2O + 2Pd$	[4]
NH_3 formation	$Pd–H + Pd–N \rightarrow Pd–NH + Pd$	[5]
	$Pd–NH + 2Pd–H \rightarrow NH_3 + 3Pd$	[6]
CO_2 formation	$Pd–CO + Pd–O \rightarrow CO_2 + 2Pd$	[7]

Reaction [1] suggests that the hydrogen pulse produced adsorbed hydrogen which reacts with adsorbed oxygen (reaction [3]) and adsorbed nitrogen (reaction [5]) (38, 39). These two reaction steps caused the Pd–N=O concentration to decrease, as shown by the decrease in Pd–N=O intensity (i.e., coverage) in Fig. 5 accompanied by an increase in NO conversion and CO_2 formation in Fig. 6c. The results in Figs. 5 and 6 show that hydrogen facilitates Pd–N=O dissociation by removal of adsorbed N and O. The results indicate that Pd–N=O is the active adsorbate involved in dissociation, producing adsorbed N and O for the reaction with adsorbed hydrogen and CO.

Figure 7 shows the MS intensity of the IR cell effluents during the H_2 pulse at different temperatures. Results for 473 K are identical to those reported in Figs. 6b and 6c. High MS intensity represents high concentration of a specific gaseous species. A significant drop in NO concentration and a marked increase in CO_2 concentration

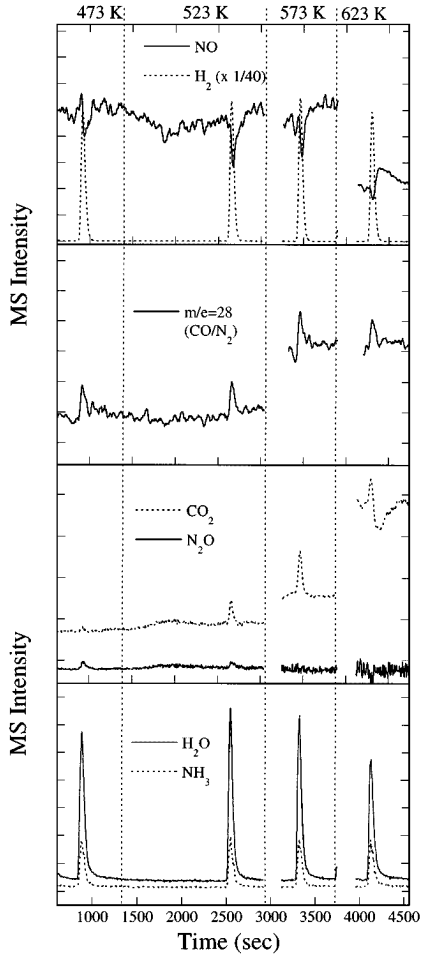

FIG. 7. MS intensity profiles of IR cell effluent during H_2 pulse at different temperatures.

between 573 and 623 K characterized the difference in the reaction rate before and after light-off. During the steady NO–CO reaction, N_2O, H_2O, and NH_3 were not formed. The reaction showed near 100% selectivity for the conversion of NO to N_2, indicating that NO conversion should be the same as that of CO. The difference in the value of NO and CO conversion in Table 1 is a result of experimental error of gas chromatographic analysis. Pulse injection of H_2 caused a decrease in NO concentration and an increase in CO_2, N_2O, H_2O, and NH_3 concentrations as shown by the MS profile. The area under the MS peak profile reflects the amount of each respective species produced during the H_2 pulse.

Careful comparison of these MS profiles shows that hydrogen pulses produced more H_2O and caused a significant increase in NO conversion at lower temperatures than at 623 K (i.e., above light-off). Temperature has little effect on NH_3 formation. N_2O was formed only at 473 and 523 K during H_2 pulses. The overlapping of the CO MS profile with the N_2 MS profile requires the use of CO_2 formation rate to infer the effect of temperature on N_2 formation during the H_2 pulse. Increase in CO_2 formation with temperature suggests an increase in CO conversion which corresponds to a reduction in the CO concentration.

Pulse O_2 into NO–CO Flow

Figure 8a shows that exposure of the catalyst to the steady-state NO/CO/He flow produced Pd–C≡O at 2083 cm^{-1}, $^{Pd}_{Pd}$>C=O at 1912 cm^{-1}, and Pd–N=O at 1754 cm^{-1}, which resemble those shown in Fig. 5a. Pulse injection of oxygen caused a reduction in the intensity of Pd–C≡O and an increase in the intensity of Pd–N=O and

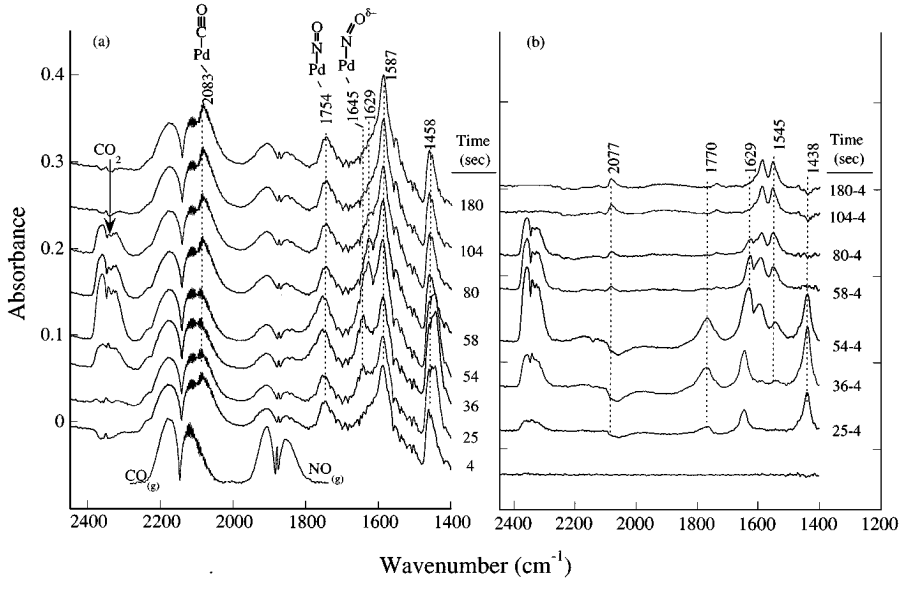

FIG. 8. (a) Transient IR spectra of adsorbed species during the 10 cm^3 O_2 pulse into the flow of NO/CO/He (3/9/28 cm^3/min) at 473 K. (b) The difference spectra from the first spectrum.

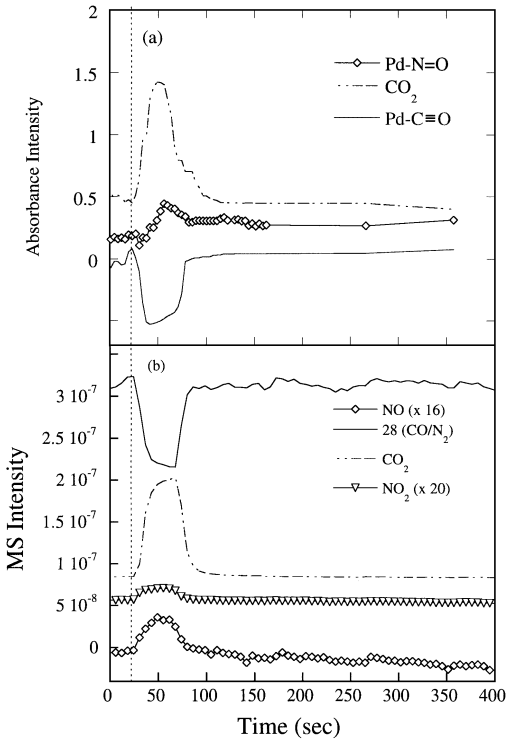

FIG. 9. (a) Integrated absorbance intensity as a function of time obtained by $\bar{A}_{CO_2} = \int_{2350}^{2387} A(v)\,dv$, $\bar{A}_{N_2O} = \int_{2229}^{2271} A(v)\,dv$, $\bar{A}_{Pd-C\equiv O} = \int_{2051}^{2106} A(v)\,dv$, and $\bar{A}_{Pd-N=O} = \int_{1718}^{1780} A(v)\,dv$. (b) MS intensity profiles of effluent from the reactor in Fig. 8 as a function of time.

gaseous CO_2 at 2364 and 2335 cm^{-1}. The presence of O_2 also led to the emergence of the Pd–N$^{\diagup O^{\delta-}}$ band at 1645 cm^{-1} after 36 s. The variation in coverage of adsorbed species is further manifested by the difference spectra in Fig. 8b. Following the O_2 pulse, Pd–C≡O increased in intensity; the catalyst activity and most adsorbates returned to their initial states.

Figure 9 shows the change in concentration of adsorbates as well as the IR cell effluent gaseous products. The CO_2 formation is accompanied by a decrease in Pd–C≡O coverage and an increase in that of Pd–N=O. The MS response of $m/e = 28$ is nearly identical to the mirror image of the CO_2 response, except for a small amount of CO that is adsorbed on the catalyst surface. Increases in the rate of CO_2 and NO_2 formation suggests occurrence of the following reaction steps:

$$Pd + O_2 \rightarrow 2Pd\text{–}O \qquad [8]$$

$$Pd\text{–}NO + Pd\text{–}O \rightarrow 2Pd + NO_2 \qquad [9]$$

$$Pd\text{–}C\equiv O + Pd\text{–}O \rightarrow 2Pd + CO_2. \qquad [10]$$

Due to the inability to observe the dynamics of adsorbed oxygen, the oxygen role in the reaction has to be inferred from how the oxygen pulse affects the concentration of IR-observable NO and CO adsorbates. Reaction [8] suggests that the oxygen pulse produced adsorbed oxygen which further reacts with adsorbed NO to form NO_2 (reaction [9]) and Pd–C≡O to form CO_2 (reaction [10]) (34). Reaction [10] is supported by the similarity in the contour of response between increases in CO_2 and decreases in Pd–C≡O concentration. In addition to participation in the oxidation reactions, a major effect of adsorbed oxygen is to increase the concentration of Pd–N=O. An increase in Pd–N=O concentration in the presence of adsorbed O indicates that adsorbed O from the O_2 pulse blocks the neighboring Pd free site required for Pd–N=O dissociation.

Figure 10a shows the IR spectra of adsorbates during the O_2 pulse at 623 K. We present this result because the

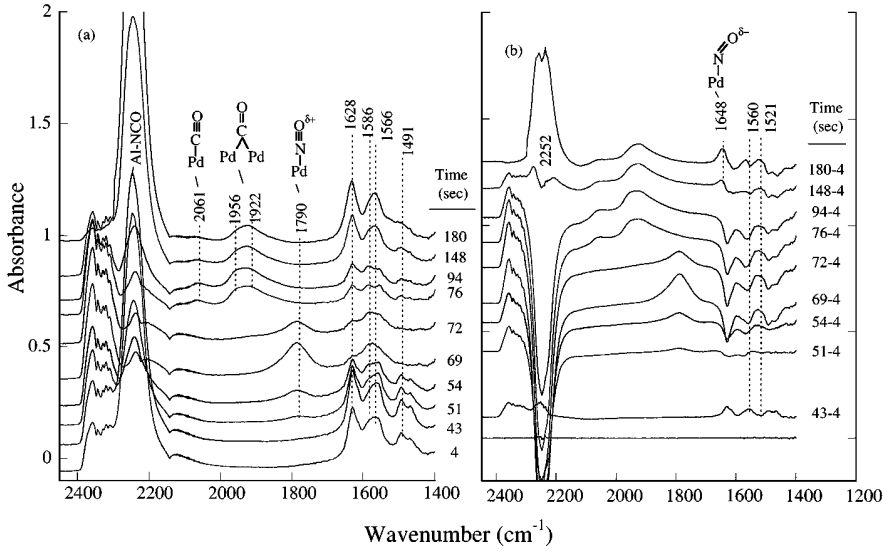

FIG. 10. (a) Transient IR spectra of adsorbed species during the 10 cm^3 O_2 pulse into the NO/CO/He (3/9/28 cm^3/min) flow at 623 K. (b) The difference spectra from the first spectrum.

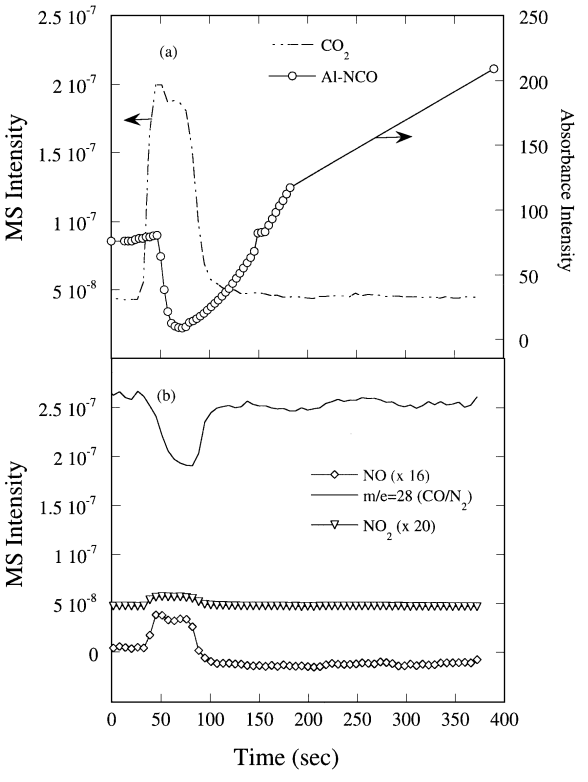

FIG. 11. (a) Integrated absorbance intensity obtained by $\bar{A}_{\text{Al–NCO}} = \int_{2183}^{2294} A(v)\,dv$ and MS intensity profiles as a function of time. (b) MS intensity profiles of effluent from the reactor in Fig. 10 as a function of time.

effect of the oxygen pulse on the behavior of adsorbates at 623 K is different from that at lower temperatures. Flowing NO/CO/He over the catalyst surface produced a weak shoulder Pd–C≡O band at 2061 cm^{-1}, a strong Al–NCO band at 2245 cm^{-1}, and nitrato and carbonate species in the 1630–1400 cm^{-1} region. Pulsing 10 cm^3 oxygen into NO/CO/He flow resulted in the following: (i) a reduction in intensity of Al–NCO, nitrato, and carbonate species; (ii) an increase in the formation of CO_2; and (iii) the appearance of the Pd–N≡$O^{\delta+}$ band at 1790 cm^{-1}. During the midpoint of the O_2 pulse, $^{Pd}_{Pd}$>C=O at 1956 and 1922 cm^{-1} as well as Pd–$N^{\diagup O^{\delta-}}$ at 1648 cm^{-1} emerged; the intensity of Al–NCO, nitrato, and carbonate species increased. Figure 11 shows that the oxygen pulse produced CO_2 and NO_2 and caused a decrease in NO conversion at 623 K. Comparison of transients of adsorbate and product concentration shows that CO_2 response leads that of Al–NCO.

DISCUSSION

The NO–CO Reaction Mechanism

The mechanism of the NO–CO reaction on Pd/Al_2O_3 can be represented by the following reaction steps (12, 17, 26):

Adsorption and desorption

Step 1 $NO + Pd \Leftrightarrow Pd–NO$

Step 2 $CO + Pd \Leftrightarrow Pd–CO$

Surface reaction

Step 3 $Pd–NO \rightarrow Pd–N + Pd–O$

Step 4 $Pd–NO + Pd–N \rightarrow Pd–N_2O + Pd$

Step 5 $Pd–CO + Pd–O \rightarrow Pd–CO_2 + Pd$

Step 6 $2Pd–N \rightarrow Pd–N_2 + Pd$

Step 7 $Pd–N_2O \Leftrightarrow Pd + N_2O$

Step 8 $Pd–CO_2 \Leftrightarrow Pd + CO_2$

Step 9 $Pd–N_2 \Leftrightarrow Pd + N_2$

Vibrational spectroscopy provided evidence for adsorption of NO and CO (i.e., steps 1, 2) and their adsorbate structure. Assignment of the structure of adsorbed NO and CO on Pd single crystal and supported Pd catalysts was widely discussed in the literature and was based on the presumed analogy in vibrational frequency between adsorbates on the metal surface and metal complexes. In this study, we found that NO was adsorbed on the Pd surface in three forms: cationic NO (Pd–N≡$O^{\delta+}$) at 1790 cm^{-1}, neutral NO (Pd–N=O) at 1748 cm^{-1}, and bent NO (Pd–$N^{\diagup O^{\delta-}}$) at 1670 cm^{-1}. The Pd–N≡$O^{\delta+}$ at 1780 cm^{-1} has been observed on oxidized Pd/Al_2O_3 catalysts (31). The band in the 1660–1750 cm^{-1} range has been observed for the NO adsorption on Pd[110], [111], and [112] sites (24, 27, 32–34). A band near 1750 cm^{-1} which emerged at high NO coverage has been attributed to the linear NO on atop sites (i.e., single atom sites). It has been suggested that increased packing in the adlayer at higher coverage causes the NO to tilt in an atop position to relieve steric repulsion (32). This 1750 cm^{-1} band has also been observed on supported Pd catalysts (19, 22, 27).

Figure 3b showed CO adsorbed in the form of linear CO (Pd–C≡O) at 2062 cm^{-1} and bridged CO ($^{Pd}_{Pd}$>C=O) at 1966–1862 cm^{-1}. Assignment of these bands is in good agreement with those reported for CO on Pd[100], [110], and [111] (24, 27) as well as supported Pd catalysts (19, 21, 23, 26, 27, 35). Coadsorption of CO and NO studies on Pd[110] at 300 K have revealed that NO adsorption destabilized $^{Pd}_{Pd}$>C=O and stabilized Pd–C≡O as shown by transformation of adsorbed CO from the $^{Pd}_{Pd}$>C=O state to the Pd–C≡O state in the presence of NO (24). Although extensive studies have been done to identify the structure of NO and CO adsorbates, little attention has been given to the study of the reactivity of these adsorbates.

Evidence for NO dissociation (i.e., step 3) has been provided by temperature-programmed desorption (TPD) studies on Pd[100] and [112] as well as supported Pd catalysts which showed that N_2 and N_2O were formed during the

TPD process (31, 33, 34). In contrast, no evidence was found for NO dissociation on Pd[110] and [111] (33, 34, 36). Knowledge of the Pd sites for the N–O bond breaking during the TPD is not sufficient for developing a comprehensive reaction mechanism since both adsorbate and surface structure of the catalyst are greatly affected by the reaction environment. The N–O bond breaking process and the adsorbate reactivity must be addressed under reaction conditions where both NO and CO reactants as well as products are present.

Results of selective enhancement and poisoning studies provided direct evidence of the dissociation of Pd–N=O to form adsorbed N and O during the NO–CO reaction. Selective enhancement of the NO–CO reaction can be achieved by the addition of hydrogen which reacts with adsorbed N and O to produce NH_3 and H_2O. Removal of adsorbed N and O caused not only a marked decrease in Pd–N=O concentration but also a significant increase in NO conversion and formation of CO_2 and N_2. The increase in NO conversion; the decrease in Pd–N=O concentration; and the increase in NH_3, H_2O, and CO_2 formation clearly support the involvement of Pd–N=O in the reaction sequence

$$NO \xrightarrow{Pd} Pd\text{–}N{=}O \xrightarrow{H_2,CO} Pd + N_2 + NH_3 + H_2O + CO_2.$$

Selective poisoning with oxygen resulted in an increase in Pd–N=O, CO_2, and NO_2 concentration and a decrease in NO conversion. Increased CO_2 and NO_2 formation during O_2 addition is expected since Pd is known for oxidation of adsorbed CO and NO. As opposed to selective enhancement, selective poisoning caused an increase in Pd–N=O concentration and a decrease in NO conversion, further confirming Pd–N=O as an active adsorbate for the NO–CO and NO–CO–H_2 reactions.

The role of adsorbed CO in the NO–CO reaction is the removal of adsorbed O from NO dissociation. However, the observed increase in Pd–C≡O intensity during hydrogen addition does not provide unambiguous evidence to determine whether Pd–C≡O participates in the reaction. As opposed to hydrogen addition, results during oxygen addition in Fig. 9 showed that the CO_2 concentration profile is the near mirror image of the concentration profile of Pd–C≡O, suggesting that Pd–C≡O is the active adsorbate involved in CO_2 formation during the NO–CO–O_2 reaction.

Both Pd–C≡O and Pd–N=O are adsorbed on atop sites. These two species appear to compete for the same type of Pd adsorption sites, as shown by their opposite trend in variation, e.g., decrease in Pd–N=O concentration accompanied by an increase in Pd–C≡O concentration during H_2 pulse, and an increase in Pd–N=O concentration accompanied by a decrease in Pd–C≡O concentration during O_2 pulse.

Variation in concentration of adsorbates, reactants, and products during selective enhancement and poisoning provides information not only for identification of active adsorbates but also for determination of the rate-determining step. The rate-determining step is often much slower than all the subsequent steps leading to products. As a result, the rate-determining step should cause the accumulation of the active adsorbates. During the NO–CO reaction at 473 K, Pd–N=O was accumulated on the surface as a result of slow rate of either NO dissociation (step 3) or oxygen removal (step 5). During the H_2 pulse, the process for removal of adsorbed oxygen is accelerated; Pd–N=O is depleted and the rate of NO conversion is increased. The whole sequence of conversion of NO/CO to N_2/CO_2 was accelerated due to increase in the rate of oxygen removal. Thus, removal of adsorbed oxygen controls the rate of the entire reaction sequence. Since the oxygen removal during the NO–CO reaction is achieved by step 5 (i.e., Pd–CO + Pd–O → Pd–CO_2 + Pd), it can be concluded that step 5 is the rate-limiting step (i.e., controlling step for the reaction). The removal of adsorbed oxygen as a rate-determining step has also been proposed for the NO–CO reaction on Rh and Pd catalysts (37, 38).

While variation in the concentration of adsorbates during the H_2 and O_2 pulses into the NO/CO flow allows elucidation of active adsorbates and the rate-determining step during the NO–CO reaction, the variation of adsorbate concentration is an indication of shift in the rate-limiting step. The H_2 pulse into NO/CO flow caused depletion of Pd–N=O, suggesting that the rate-determining step shifts from removal of adsorbed oxygen (step 5) to diffusion of gaseous NO into the catalyst pores. During the H_2 pulse, the rate of NO diffusion is not high enough to supply NO for reaction with CO and H_2 on the catalyst surface. In contrast to the H_2 pulse, the O_2 pulse produced adsorbed oxygen, further slowing down the removal of adsorbed oxygen and causing accumulation of Pd–N=O.

It is worth noting that Al–NCO exhibited a prominent IR band at 623 K. It has been shown that this species is produced from the following steps (18, 39).

$$M^0\text{–N} + M^0\text{–CO} \rightarrow M^0\text{–NCO} + M^0$$

$$M^0\text{–NCO} + \text{Al} \rightarrow M^0 + \text{Al–NCO};$$

M^0 is the reduced metal site which includes Rh, Pd, Ru, and Pt.

The Al–NCO species has been considered as a spectator for the CO_2 formation by our previous ^{13}CO isotopic tracing studies (12). The characteristic of Al–NCO can be revealed by comparison of its transient response with those of other adsorbates and gaseous products in Fig. 11. Response of CO_2 leads that of Al–NCO, indicating that adsorbed oxygen is more reactive toward adsorbed CO to form CO_2 than with Al–NCO. The gradual Al–NCO recovery, after O_2 left the reactor, may be due to the slow transfer of NCO from metal sites to the Al_2O_3 surface.

CONCLUSIONS

Infrared spectra of the NO–CO reaction on Pd/Al_2O_3 show that NO adsorbs as Pd–N≡$O^{\delta+}$, Pd–N=O, and Pd–N$^{\diagup O^{\delta-}}$ while CO adsorbs as Pd–C≡O and $^{Pd}_{Pd}$>C=O. These observations are in good agreement with numerous vibrational spectroscopy studies which provide information about the structure of NO and CO adsorbates and their interactions (19, 21–30). The current investigation is concerned with the crucial issue of distinguishing active adsorbates from spectator adsorbates using a novel *in situ* IR coupled with a selective enhancement and poisoning technique. This technique measured the nature of the specific adsorbate involved in the NO dissociation and the reaction for CO_2 formation. Knowledge of NO–H_2, NO–CO–H_2, and NO–CO–O_2 reactions allows selection of H_2 as a reaction enhancer and O_2 as a poison for the NO–CO reaction (40–43). Addition of H_2 into the NO/CO flow produced adsorbed H which reacts with adsorbed N and adsorbed O to form NH_3 and H_2O as shown in Fig. 1b. Removal of adsorbed N and O caused not only a marked decrease in Pd–N=O but also a significant increase in NO conversion. Addition of O_2 into the NO–CO flow produced adsorbed oxygen which inhibits N–O dissociation, resulting in accumulation of Pd–N=O and a decrease in NO conversion, as shown in Fig. 1c. Variation in adsorbate as well as reactant/product concentrations during selective enhancement and poisoning suggests that Pd–N=O and Pd–C≡O are the active adsorbates involved in the NO–CO reaction on Pd/Al_2O_3.

This study demonstrates the usefulness of the *in situ* IR-selective enhancement/poisoning technique in identification of active adsorbate for the NO–CO reaction. Selection of a poison appears to be easier than that of a reaction enhancer since various poisons have been identified in extensive catalytic deactivation studies.

ACKNOWLEDGMENT

The authors gratefully acknowledge the support of this research by the National Science Foundation under Grant C TS-942111996.

REFERENCES

1. Delgass, W., Haller, G., Kellerman, R., and Lundford, J., "Spectroscopy in Hetrogeneous Catalysis." Academic Press, New York, 1979.
2. Tamaru, K., *in* "Catalysis: Science and Technology" (J. R. Anderson and M. Boudart, Eds.), Vol. 9, p. 87. Springer-Verlag, Berlin/Heielberg/New York, 1991.
3. Rabo, J., *in* "Proceedings, 10th International Congress on Catalysis, Budapest, 1992" (L. Guczi, F. Solymosi, and P. Tetenyi, Eds.), Part A, p. 1. Akadémiai Kiadó, Budapest, 1993.
4. Bell, A. T., and Hair, M. L., Eds., "Vibrational Spectroscopies for Adsorbed Species," ACS Symposium Series, Vol. 137. Am. Chem. Soc., Washington, DC, 1980.
5. Davydov, A., *in* "Infrared Spectroscopy of Adsorbed Species on the Surface of Transition Metal Oxides" (C. H. Rochester, Ed.). Wiley, Chichester, England, 1990.
6. Yates, J. T., Jr., and Madey, T. E., Eds., "Vibrational Spectroscopy of Molecules on Surfaces." Plenum Press, New York, 1987.
7. Dalla Betta, R. A., and Shelef, M., *J. Catal.* **48**, 111 (1977).
8. Hecker, W. C., and Bell, A. T., *J. Catal.* **84**, 200 (1983).
9. Pien, S. I., and Chuang, S. S. C., *J. Mol. Catal.* **68**, 313 (1991).
10. Kaul, D. L., and Wolf, E. E., *J. Catal.* **89**, 348 (1984).
11. Li, Y. E., and Conzalez, R. D., *Catal. Lett.* **1**, 229 (1988).
12. Krishnamurthy, R., Chuang, S. S. C., and Balakos, M. W., *J. Catal.* **157**, 512 (1995).
13. Efstathiou, A. M., and Bennett, C. O., *J. Catal.* **120**, 137 (1989).
14. Krishna, K. R., and Bell, A. T., *J. Catal.* **139**, 104 (1993).
15. Shannon, S. L., and Goodwin, J. G., Jr., *Chem. Rev.* **95**, 677 (1995).
16. Belton, D. N., and Schmieg, S. J., *J. Catal.* **144**, 9 (1993).
17. Taylor, K. C., *Catal. Rev. Sci. Eng.* **35**, 457 (1993).
18. Krishnamurthy, R., and Chuang, S. S. C., *J. Phys. Chem.* **99**, 16727 (1995).
19. Grill, C. M., and Gonzalez, R. D., *J. Phys. Chem.* **84**, 878 (1980).
20. Chuang, S. S. C., Brundage, M. A., Balakos, M. W., and Srinivas, G., *Appl. Spectrosc.* **49**, 1151 (1995).
21. Palazov, A., Chang, C. C., and Kokes, R. J., *J. Catal.* **36**, 338 (1975).
22. Moriki, S., Inoue, Y., Miyazki, E., and Yasumori, I., *J. Chem. Soc. Faraday Trans. 1* **78**, 171 (1982).
23. Kikuzono, B. Y., Kagami, S., Naito, S., Onishi, T., and Tamaru, K., *Faraday Discuss. Chem. Soc.* **72**, 135 (1982).
24. Raval, R., Blyholder, G., Haq, S., and King, D. A., *J. Phys. Condensed Matter* **1**, SB165 (1989).
25. Duplan, J. L., and Praliaud, H., *in* "Catalysis and Automotive Pollution Control II" (A. Crucq, Ed.), p. 667. Elsvier, Amsterdam, 1991.
26. Elhamdaoui, A., Bergeret, G., Massardier, J., Primet, M., and Renouprez, A., *J. Catal.* **148**, 47 (1994)
27. Xu, X., Chen, P., and Goodman, D. W., *J. Phys. Chem.* **98**, 9242 (1994).
28. Hoost, T. E., Otto, K., and Laframboise, K. A., *J. Catal.* **155**, 303 (1995).
29. Nakamoto, K., "Infrared and Raman Spectra of Inorganic and Coordination Compounds." Wiley, New York, 1986.
30. Terenin, A., and Roev, L., *Spectrochim. Acta.* **11**, 946 (1959).
31. Valden, M., Keiski, R. L., Xiang, N., Pere, J., Aaltonen, J., Pessa, M., Maunula, T., Savimaki, A., Lahti, A., and Harkonen, M., *J. Catal.* **161**, 614 (1996).
32. Raval, R., Harrison, M. A., Haq, S., and King, D. A., *Surf. Sci.* **294**, 10 (1993).
33. Sugai, S., Watanabe, H., Kioka, T., Miki, H., and Kawasaki, K., *Surf. Sci.* **259**, 109 (1991).
34. Ramsier, R. D., Gao, Q., Waltenburg, H. N., Lee, K. W., Nooij, O. W., Lefferts, L., and Yates, J. T., Jr., *Surf. Sci.* **320**, 209 (1994).
35. Pavlova, S. N., Sadykov, V. A., Razdobarov, V. A., and Paukshtis, E. A., *J. Catal.* **161**, 507 (1996).
36. Conrad, H., Ertl, G., Kuppers, J., and Latta, E. E., *Surf. Sci.* **65**, 235 (1977).
37. Cho, B. K., Shanks, B. H., and Bailey, J. E., *J. Catal.* **115**, 486 (1989).
38. Rainer, D. R., Koranne, M., Vesecky, S. M., and Goodman, D. W., *J. Phys. Chem.* **101**, 10769 (1997).
39. Unland, M. L., *J. Catal.* **31**, 459 (1973).
40. Mergler, Y. J., and Nieuwenhuys, B. E., *Appl. Catal. B* **12**, 95 (1997).
41. Hecker, W. C., and Bell, A. T., *J. Catal.* **88**, 289 (1984).
42. Oh, S. H., and Carpenter, J. E., *J. Catal.* **101**, 114 (1986).
43. Graham, G. W., Logan, A. D., and Shelef, M., *J. Phys. Chem.* **97**, 5445 (1993).